The AMBRE Project: Origin and evolution of sulfur in the Milky Way

J. Perdigon, P. de Laverny, A. Recio-Blanco, E. Fernandez-Alvar, P. Santos-Peral, G. Kordopatis, M. A. Álvarez

A&A 647, A162 (2021)
https://doi.org/10.1051/0004-6361/202040147

Astronomy & Astrophysics

The AMBRE Project: Origin and evolution of sulfur in the Milky Way*

J. Perdigon[1,**], P. de Laverny[1], A. Recio-Blanco[1], E. Fernandez-Alvar[1], P. Santos-Peral[1], G. Kordopatis[1], and M. A. Álvarez[2]

[1] Université Côte d'Azur, Observatoire de la Côte d'Azur, CNRS, Laboratoire Lagrange, Bd de l'Observatoire, CS 34229, 06304 Nice cedex 4, France
e-mail: laverny@oca.eu
[2] CIGUS -CITIC- Department of Computer Science and Information Technologies, University of A Coruña, A Coruña, Spain

Received 16 December 2020 / Accepted 14 January 2021

ABSTRACT

Context. Sulfur is a volatile chemical element that plays an important role in tracing the chemical evolution of the Milky Way and external galaxies. However, its nucleosynthesis origin and abundance variations in the Galaxy are still unclear because the number of available stellar sulfur abundance measurements is currently rather small.
Aims. The goal of the present article is to accurately and precisely study the sulfur content of large number of stars located in the solar neighbourhood.
Methods. We use the parametrisation of thousands of high-resolution stellar spectra provided by the AMBRE Project, and combine it with the automated abundance determination GAUGUIN to derive local thermodynamic equilibrium sulfur abundances for 1855 slow-rotating FGK-type stars. This is the largest and most precise catalogue of sulfur abundances published to date. It covers a metallicity domain as high as ∼2.5 dex starting at [M/H] ∼ −2.0 dex.
Results. We find that the sulfur-to-iron abundances ratio is compatible with a plateau-like distribution in the metal-poor regime, and then starts to decrease continuously at [M/H] ∼ −1.0 dex. This decrease continues towards negative values for supersolar metallicity stars as recently reported for magnesium and as predicted by Galactic chemical evolution models. Moreover, sulfur-rich stars having metallicities in the range [−1.0, −0.5] have very different kinematical and orbital properties with respect to more metal-rich and sulfur-poor ones. Two disc components, associated with the thin and thick discs, are thus seen independently in kinematics and sulfur abundances. The sulfur radial gradients in the Galactic discs have also been estimated. Finally, the enrichment in sulfur with respect to iron is nicely correlated with stellar ages: older metal-poor stars have higher [S/M] ratios than younger metal-rich ones.
Conclusions. This work has confirmed that sulfur is an α-element that could be considered to explore the Galactic populations properties. For the first time, a chemo-dynamical study from the sulfur abundance point of view, as a stand-alone chemical element, is performed.

Key words. Galaxy: abundances – Galaxy: evolution – stars: abundances

1. Introduction

Sulfur is a chemical species of particular importance in the context of stellar nucleosynthesis and the chemical evolution of galaxies. It is a volatile element and, as a consequence, it is not blocked into the dust grains of the interstellar medium (ISM). It is therefore a good tracer of the chemical evolution of galaxies, in particular at large redshifts (Savage & Sembach 1996). Moreover, from the stellar nucleosynthesis point of view, sulfur is classified as an α-element (e.g., oxygen, magnesium, titanium, ...). It is indeed produced via α-capture in the inner layers of massive stars (see e.g., Woosley & Weaver 1995; Nomoto et al. 2013). These chemical species are then released into the ISM mostly through Type II supernovae on a relatively short timescale. It is therefore believed that the abundance of all these α-elements approximately follows the same behaviour during the Galactic chemical evolution. On the other hand, although also partly produced in massive stars, iron is mostly produced and expelled into the ISM by Type Ia supernovae on a much longer timescale. Thus, we expect that the [α/Fe] ratio (and thus [S/Fe]) remains almost constant with respect to iron content in the metal-poor regime (i.e., as a plateau), corresponding to the epoch before the ignition of the first Type Ia supernovae. Then, this ratio is expected to decrease afterwards as soon as the amount of released iron increases with time. Adopting such production sites, Galactic chemical evolution models quite successfully reproduce the main observed behaviour of sulfur and other α-elements as a function of the metallicity (among other recent studies, see Prantzos et al. 2018; Grisoni et al. 2017; Palla et al. 2020), confirming that the major production site of S is indeed Type II supernovae.

On the observational side, a few studies have reported sulfur abundance enhancements in the metal-poor regime. Francois (1988) was the first to suspect the α-like behaviour of sulfur for [Fe/H] < −1 dex with a plateau-like structure, and this was then confirmed by later studies (see e.g., Ryde & Lambert 2004; Nissen et al. 2004, 2007; Spite et al. 2011; Kacharov et al. 2015). These works invalidated the

* Full Tables 5 and 6 are only available at the CDS via anonymous ftp to cdsarc.u-strasbg.fr (130.79.128.5) or via http://cdsarc.u-strasbg.fr/viz-bin/cat/J/A+A/647/A162
** Send offprint requests to Patrick de Laverny.

suggestion of Israelian & Rebolo (2001) who found a steady increase in [S/Fe] with decreasing metallicities, leading to some suspected extreme sulfur-rich stars ([S/Fe] ≈ 0.8 dex at [Fe/H] < −2.0 dex). The plateau of sulfur in the metal-poor regime nonetheless appears with a large dispersion mainly caused by the difficulty of analysing weak lines at these low metallicities. At higher but still subsolar metallicities (−1.0 dex ≲ [Fe/H] ≲ 0.0 dex), and as expected for any α-element, the decline of [S/Fe] with metallicity in the Galactic disc is clearly observed and interpreted as the release of iron from Type Ia SNe at [Fe/H] ≲ −1 dex (see e.g., Chen et al. 2002; Caffau et al. 2005; Ryde 2006; Matrozis et al. 2013). This therefore supports the idea of a common nucleosynthetic origin for sulfur and other α -species.

It is interesting to note that all these studies rely on rather small samples of stars (typically a few tens). However, in order to be able to study possible different sulfur content in the various Galactic populations, large statistics is necessary. This changed recently thanks to a few studies. First, Luck (2015) reported SI abundances of ∼1100 G-K giants but with rather large uncertainties and dispersions in [S/Fe]. Moreover, a strong temperature dependency, probably caused by blending from unknown lines, caused blurring in the main picture. Then, Takeda et al. (2016) derived sulfur abundances for up to ∼400 dwarfs and giants, confirming the decrease in [S/Fe] with metallicity. Later on, within the *Gaia*-ESO Survey, Duffau et al. (2017) managed to derive sulfur abundances for a sample of 1301 Galactic stars, including stars in open and globular clusters, but with only half a dozen stars below [M/H] ∼ −1.0 dex. Although the global behaviour is again partially blurred by rather large measurement dispersions and temperature-dependent derived abundances, this study seems to confirm the α-like behaviour of sulfur at subsolar metallicities (−1 ≲ [M/H] ≲ 0 dex). Finally, Costa Silva et al. (2020, hereafter CS20) recently presented a precise analysis of sulfur in 719 stars of the solar neighbourhood having metallicities higher than −1.0 dex. This work clearly showed that sulfur behaves like a typical α-element in the thin and thick discs, in rather good agreement with the literature models of Galactic sulfur evolution (Romano et al. 2010; Kobayashi et al. 2011; Prantzos et al. 2018).

In the present study we profit from the spectra parametrised within the AMBRE Project de Laverny et al. (2013) and provided by the ESO archives of the HARPS, FEROS, and UVES spectrographs. We estimated precise and homogeneous sulfur abundances for a catalogue containing an unprecedented number of stars, having metallicities varying from ∼−2.0 dex to ∼+0.7dex. This allowed us to depict a global and homogeneous view of sulfur in the main Galactic components. The paper is structured as follows. We present in Sect. 2 the method developed for automatically deriving the sulfur abundances. The AMBRE-sulfur catalogue of almost 1,855 stars is then presented in Sect. 3. In Sect. 4, we discuss the sulfur behaviour in the solar vicinity in terms of abundance variations, stellar kinematics and ages, and Galactic radial gradients. We finally summarise our results in Sect. 5.

2. Derivation of the AMBRE sulfur abundances

This study has been carried out in the framework of the AMBRE Project (de Laverny et al. 2013), whose first aim was to derive the main atmospheric parameters (effective temperature $T_{\rm eff}$, surface gravity $\log(g)$, mean metallicity [M/H], and enrichment in α -elements with respect to iron [α/Fe]) of ESO archived spectra. This is performed thanks to the MATISSE algorithm (Recio-Blanco et al. 2006) trained with a specific grid of synthetic spectra (de Laverny et al. 2012). For the present analysis, we also use other AMBRE data products (for a detailed description, see Worley et al. 2012) as the stellar radial velocity ($V_{\rm Rad}$), the signal-to-noise ratio (S/N), the full width at half maximum (FWHM) of the cross-correlation function (CCF) used to estimate $V_{\rm Rad}$ (i.e., an estimate of the typical width of the lines, therefore including the effects of the rotational velocity), and a quality flag of the stellar parametrisation (based on the computation of a χ^2 between the observed and reconstructed spectra at the derived stellar parameters).

From these parametrised AMBRE spectra the sulfur abundances were then derived thanks to GAUGUIN, an optimisation method coupling a precomputed grid of synthetic spectra (see Sect. 2.2 for a description of this grid) and a Gauss-Newton algorithm. GAUGUIN was originally developed in the framework of the *Gaia*/RVS analysis within the *Gaia*/DPAC for the estimation of the stellar atmospheric parameters: for the mathematical basis, see Bijaoui et al. (2010); and then, the first applications in Bijaoui et al. (2012) and Recio-Blanco et al. (2016). A natural and simple extension of GAUGUIN's applicability to the derivation of stellar chemical abundances was then initiated within the context of the *Gaia*/RVS (DPAC/Apsis pipeline, Bailer-Jones et al. 2013), the AMBRE Project and the *Gaia*-ESO Survey. We first published a detailed description of the application of GAUGUIN for the derivation of chemical abundances within the AMBRE context in Guiglion et al. (2016). We also refer to Sect. 2.2 for its specific application to sulfur abundances.

2.1. Adopted line list and computation of the grid of reference synthetic spectra

For the selection of our analysed sulfur lines, we refer to the works of Caffau et al. (2005), Duffau et al. (2017), and Takeda et al. (2016) who studied multiplets 1, 6, and 8 (respectively at ≈922, 869, and 675 nm). Taking into account (i) the wavelength ranges covered by our observed spectra (see Sect. 2.2), (ii) the strength of these SI multiplets in FGK star spectra, (iii) the existence of almost blend-free spectral ranges, and (iv) the expected weak non-local thermodynamic equilibrium (NLTE) effects (see below), we selected the lines of multiplet 8 for the present analysis. It is known that these lines are almost unaffected by NLTE effects since they are formed in deep atmospheric layers (Korotin 2009). For example, Takeda et al. (2016) and Korotin et al. (2017) have shown that NLTE departures should always be smaller than 0.1 dex for our sample stars.

For the present analysis of the multiplet 8 lines the atomic data of Wiese et al. (1969) were adopted and are reported in Table 1. We note that we have found a small systematic bias in the abundances derived from the 674.8 nm line with respect to the two others. This could reflect some possible small uncertainties in the atomic data adopted for the three components of this line (see Sect. 2.3.3). The proposed correction for the $\log gf$ (+0.08 dex) of these 674.8 nm transitions would agree closely with the line data of Biemont et al. (1993).

From these adopted SI lines completed by all the molecular and atomic linelists of Heiter et al. (2021), we computed a grid of synthetic spectra around the selected SI lines thanks to the TURBOSPECTRUM code (Plez 2012) and the MARCS model atmospheres (Gustafsson et al. 2008) under the LTE, 1D, and hydrostatic assumptions, adopting the Grevesse et al. (2007) solar chemical composition. For this specific sulfur grid, we followed a similar, but slightly updated, procedure as in de Laverny et al. (2012). The ranges of the

Table 1. Adopted multiplet 8 sulfur line data (Wiese et al. 1969).

Line(nm)	χ_e(eV)	$\log gf$
674.3440	7.866	−1.27
674.3531	7.866	−0.92
674.3640	7.866	−1.03
674.8573	7.868	−1.39 (*)
674.8682	7.868	−0.80 (*)
674.8837	7.868	−0.60 (*)
675.6851	7.870	−1.76
675.7007	7.870	−0.90
675.7171	7.870	−0.31

Notes. (*)Probably underestimated, see text.

atmospheric parameters are $4000 \leq T_{\rm eff} \leq 8000$ K (in steps of 250 K), $+0.0 \leq \log(g) \leq +5.5$ (in steps of 0.5, g being in cm s^{-2}), and $-5.0 \leq$ [M/H] $\leq +1.0$ dex (with steps of 0.5 dex for metallicities smaller than −1.0 dex and 0.25 dex above); up to 13 values of [α/Fe] were considered for each value of [M/H] depending on the availability of the MARCS models (with steps of 0.1 dex). Therefore, 25 961 MARCS model atmospheres with an [α/Fe] enhancement consistent with that adopted when computing the synthetic spectra were considered. Then, for each combination of these four atmospheric parameters, we computed spectra by varying sulfur abundances between $-3.0 \leq$ [S/H] $\leq +2.0$ dex with a step of 0.2 dex (i.e., 26 different values of [S/H]). The adopted sulfur solar abundance is $A_{\rm S} = 7.12$ (Scott et al. 2015). For these computations, we also adopted a micro-turbulence velocity that varies with $T_{\rm eff}$, $\log(g)$, and [M/H] following the prescription of the *Gaia*-ESO Survey (version 2 of the GES empirical relation based on microturbulence velocity determinations from literature samples; Bergemann et al., in prep.). The adopted micro-turbulence velocities vary from 0.6 to 4.8 km s^{-1}, depending on the stellar parameters. We also recall that no stellar rotation is considered when computing the grid spectra. Finally, the reference AMBRE sulfur grid consists in about 675 000 spectra, covering the wavelength range from 672 to 677 nm with a wavelength step of 0.0005 nm.

2.2. Chemical analysis of AMBRE: HARPS, UVES, FEROS spectra

Our data consists of a collection of about 100 000 ESO archived spectra from the FEROS, HARPS, and UVES spectrographs, already parametrised within the AMBRE Project (see Worley et al. 2012, De Pascale et al. 2014 and Worley et al. 2016, respectively). The number of selected spectra having a S/N higher than 20 and a quality flag for their AMBRE parametrisation equal to 0 or 1 (i.e., good or very good parametrisation; see the above AMBRE papers), together with their atmospheric parameter ranges and their mean signal-to-noise ratio is summarised in Table 2. We note that two UVES setups cover the selected SI multiplet 8 lines, and are thus identified as two separate spectrographs.

In order to be analysed with our GAUGUIN pipeline in a homogeneous way, the observed spectra were first corrected by their radial velocity. Then, the spectral resolutions of the HARPS and FEROS spectra were degraded to the UVES value ($R \sim 40\,000$). We adopted a sampling wavelength step of 0.005 nm for the whole dataset in order to fulfil the Nyquist-Shannon criteria. The reference grid spectra was convolved and re-sampled accordingly.

Then, the prepared 99 271 spectra were ingested into our chemical analysis pipeline. The spectra are first automatically normalised by comparing a synthetic and an observed spectrum over a ∼7 nm domain, centred on each sulfur line. Then, the normalisation is refined over a ∼0.4 nm interval around each line (for more details on the normalisation procedure, see Santos-Peral et al. 2020a). For each of these spectra, the three components of the SI multiplet 8 in Table 1 are then analysed independently by comparing the observed and reference grid line profiles over domains covering 0.06 nm, 0.05 nm, and 0.08 nm, centred at the SI 674.3, 674.8, and 675.7 nm lines, respectively. We end up with a catalogue of about 300 000 sulfur measurements, including several non-detection and upper limit measurements.

2.3. Construction of the AMBRE-sulfur catalogue

The AMBRE-sulfur catalogue that is presented and discussed in the next sections was built as follows. We first note that our dataset contains, for some stars, a large number of repeated spectra (hereafter called 'repeats'). We thus describe below how we derived sulfur abundances from the analysis of several repeats of the same star from which up to three distinct lines can be measured.

2.3.1. Cross-match with the *Gaia* DR2 and adopted ID

The AMBRE spectra were collected with quite different instruments. The available spectra may therefore contain heterogeneous names of targets and accuracy of coordinates. The first step was thus to identify the corresponding observed stars, and in particular the identification of the spectra belonging to the same star. For this purpose we made use of the *Gaia* DR2 catalogue (Gaia Collaboration 2018) and adopted, when found, the *Gaia* DR2 ID. We refer to a forthcoming article for the detailed presentation of this cross-match between the *Gaia*/DR2 and the AMBRE catalogues. Briefly, this cross-match was performed using the stellar spectra coordinates and different checks between the derived AMBRE atmospheric parameters, $T_{\rm eff}$ estimated from ground based photometry (2MASS and APASS, Skrutskie et al. 2006; Henden et al. 2018), and *Gaia* data (e.g., G-magnitude, $B_P - R_P$ colours, $T_{\rm eff}$, radial velocities, but for more details, see also Santos-Peral et al. 2020b). We were able to identify 5076 distinct stars from the 99,271 AMBRE spectra. There is also a significant fraction (∼20%) of our spectra for which no *Gaia* DR2 ID were found. Several of these spectra actually correspond to bright stars, absent from the *Gaia*/DR2 catalogue. In this case, we simply looked in Simbad for stars having coordinates similar to the AMBRE coordinates within a radius of 10″ and consistent parametrisation. We then adopted for them the corresponding name in the Henry Draper catalogue as an ID, adding about 200 more stars into the initial sample.

Finally, among the identified stars, a significant part has several repeats: about ∼20% of the stars have more than ten repeats, and more than ten stars have more than 1000 associated spectra. Such a large number of repeats allowed us to derive sulfur abundances with very low internal uncertainties (see below).

2.3.2. Selection of the best analysed spectra

For a given star, we decided to only keep the repeats with a very consistent set of stellar parameters among each other. We therefore rejected the spectra that depart too much from the median

Table 2. Summary of the parameter ranges covered by our selected AMBRE spectra having a signal-to-noise ratio higher than 20.

Spectrograph	Number of spectra	$T_{\rm eff}$(K)	$\log(g)$(g in cm s^{-2})	[M/H](dex)	[α/Fe](dex)	$\langle S/N \rangle$	$\sigma(S/N)$
HARPS	88 178	[4015, 7620]	[1.02, 4.95]	[−3.43, 0.61]	[−0.39, 0.59]	74	29
FEROS	5821	[4000, 7623]	[1.00, 4.99]	[−3.49, 0.95]	[−0.38, 0.65]	98	52
UVES/Red580	3533	[3668, 7575]	[1.10, 5.00]	[−3.47, 0.72]	[−0.33, 0.50]	192	89
UVES/Red860	1739	[3584, 7787]	[0.00, 4.82]	[−3.49, 0.75]	[−0.39, 0.79]	157	51

values of all repeats. The threshold was arbitrarily chosen to be 1 km s^{-1}, 100 K, 0.5, 0.10 dex, and 0.05 dex for $V_{\rm rad}$, $T_{\rm eff}$, $\log(g)$, [M/H], and [α/Fe], respectively. A unique threshold can be adopted for any spectrum since we recall that the AMBRE parametrisation was performed at a constant spectral resolution for the three considered ESO spectrographs. We also note that such a rejection procedure could help to reject possible spectroscopic binaries for which their stellar parameters may seem to vary between different epochs of observation.

On the other hand, the GAUGUIN pipeline was not able in some cases to derive a useful sulfur abundance. This directly results from either a low spectrum quality (photon noise and/or cosmic rays) or from some atmospheric parameter limitations in the synthetic grid. For example, in the present analysis the reference grid is only valid for low-rotation stars. However, the AMBRE parametrisation provides an indication of the line broadening (and hence of the rotational velocity, among other broadening mechanisms) thanks to the FWHM of the cross-correlation functions derived during the radial velocity measurement. Therefore, in order to reject stars whose rotational and/or macroturbulent velocities were possibly too high, we systematically rejected all the spectra with a $FWHM_{\rm CCF} > 15$ km s^{-1} for the three spectrographs, in agreement with previous estimates (see e.g., Guiglion et al. 2016). This value corresponds to rotational velocities typically lower than ∼10–15 km s^{-1} (depending on the stellar types) at the working spectral resolution.

Moreover, for each analysed spectrum and detected sulfur lines, we also computed the lowest abundance (upper limit) that could be estimated from their atmospheric parameters and signal-to-noise ratio. We systematically rejected all the derived abundances that were lower than or too close to twice this upper limit.

Finally, all these different criteria led to the rejection of about 2/3 of the measured sulfur lines, leading to about 100 000 useful measurements of one of the three multiplet 8 sulfur lines.

2.3.3. Mean sulfur abundances and atmospheric parameters per star

We recall that our final working sample consists of 5275 distinct stars, of which the vast majority possess repeat spectra; each of them could have up to three measured lines. Our method for determining the sulfur abundance of a given star consists of two steps: (i) determining separately the mean abundance of the three sulfur lines for the available repeats and (ii) estimating the final sulfur abundance of each star by averaging up to three available mean individual abundances from the previous step. In both stages the same averaging method is employed, following the work of Adibekyan et al. (2015, hereafter A15). These authors investigated different methods of combining abundances extracted from different lines of a given element, and we adopted their weighted mean (WM) procedure to estimate our sulfur abundances. We briefly describe below the adopted methodology, and refer to A15 for more details.

For a set of N sulfur abundances [S/H]$_i$ the adopted WM is

$$[\mathrm{S/H}] = \frac{\sum_{i=1}^{N} W_i\,[\mathrm{S/H}]_i}{\sum_{i=1}^{N} W_i}, \quad (1)$$

with W_i being *weights* defined below. As shown by A15, this WM procedure has the advantage of successfully removing the effect of outliers on the final abundance, without using any ad hoc sigma-clipping procedure. The definition of the weights is based on the distance (in terms of standard deviation, std) between the available abundances and their median (med):

$$W_i = \frac{1}{\mathrm{dist}_i}; \quad \mathrm{dist}_i = \frac{[\mathrm{S/H}]_i - \mathrm{med}\,\{[\mathrm{S/H}]\}}{\mathrm{std}\,\{[\mathrm{S/H}]\}}. \quad (2)$$

In practice, if more than half of the repeats have the same abundance value, and if the abundance distribution is Gaussian, the associated median of the absolute deviation (MAD), and hence the standard deviation, could be equal to zero, resulting in an infinite weight. To circumvent this effect we decided, as suggested by A15, to bin the dist$_i$ in boxes having a width equal to 0.5. For example, all the abundances with dist$_i \leq 0.5$ will have the same weight (1/0.5 = 2 in this example).

We first applied this procedure independently for the three sulfur lines (step (i) above), hence providing their WM abundance. The final sulfur abundance (step (ii) above) estimated when more than one sulfur line was measured is also obtained with the same procedure. However, we note that if only two SI lines are available, we provide their WM final abundance only if an abundance of the strongest SI 675.7 nm component (and easiest line to analyse) is available. If only one line has been measured for a given star, we accept its [S/H] only if it comes from the 675.7 nm component. Finally, each line abundance is associated with an error Δ[S/H], proportional to the MAD amongst the repeats of the line. We adopted $\Delta[\mathrm{S/H}] = 1.483 \times \mathrm{MAD}(\{[\mathrm{S/H}]_i\})$, i.e., the scaled MAD (corresponding to a 1σ threshold for a Gaussian distribution).

We note that the atmospheric parameters (including the S/N) associated with a given star have been averaged by adopting the same WM procedure. The mean dispersions associated with these means are equal to 6 K, 0.01, 0.006 dex, and 0.004 dex for $T_{\rm eff}$, $\log(g)$, [M/H], [α/Fe], respectively. We also specify that the final sulfur abundance mean was performed after the 674.8 nm line was corrected for a systematic bias of −0.08 dex in [S/H] that could be associated with the non-calibrated line data (see Sect. 2.1). We validated our whole analysis procedure (including the line atomic data) by estimating the solar sulfur abundance derived thanks to a very high-S/N HARPS spectrum of Vesta and the solar FTS spectra of Wallace et al. (2011). For both spectra degraded at $R \sim 40\,000$, we obtained [S/H] = −0.04 dex after correcting the 674.8 nm line. Such a small bias was also seen in other reference stars (assuming [S/α]=0 for these stars). We therefore calibrated all our final abundances by this small amount of −0.04 dex in order to be consistent with the previously adopted solar sulfur abundances of Scott et al. (2015).

Table 3. Sensitivities of the sulfur abundances (in dex) caused by typical uncertainties on the stellar atmospheric parameters.

	Cool giant $T_{\rm eff} \sim 4500$ K	Cool dwarf $T_{\rm eff} \sim 5000$ K	Solar-type $T_{\rm eff} \sim 5800$ K	Hot dwarf $T_{\rm eff} \sim 6500$ K
$\Delta\, T_{\rm eff} = \pm 120$ K	±0.20	±0.20	±0.05	±0.03
Δ log(g) = ±0.25 dex	±0.07	±0.05	±0.05	±0.04
Δ [M/H] = ±0.10 dex	±0.01	±0.02	±0.02	±0.02
Total (quadratic sum)	±0.21	±0.21	±0.07	±0.05

Table 4. Typical internal uncertainties (sulfur abundance scatters, in dex) for different stellar types and S/N bins.

	Cool giant		Cool dwarf		Hot dwarf	
S/N	~40	~200	~40	~100	~80	~140
SI 674.3	–	–	0.06	0.06	0.05	0.02
SI 674.8	–	–	0.04	0.03	0.02	0.02
SI 675.7	0.03	0.03	0.06	0.04	0.02	0.02

Notes. These numbers refer to a single line in one spectrum. Since the final reported abundances are obtained by averaging up to three SI lines and several repeat spectra (when available), the actual relative uncertainties from star to star are much smaller. Only the SI 675.7 nm line can be safely analysed in cool giants.

Finally, the uncertainties were then estimated using again this WM procedure, adopting the same weights as those adopted for the final abundance. If no repeats are available for some stars, the final errors were estimated from the dispersion between the abundance of the accepted individual lines. Therefore, no dispersions are reported for stars having only one available spectra in which only one line has been measured (the SI 675.7 nm component).

2.3.4. Uncertainties associated with the derived sulfur abundances

Several sources of uncertainties can affect an abundance determination. Moreover, looking at their different significances can help to flag the reported abundances and clean the sample for future scientific exploitation.

Firstly, we estimated the sensitivity of the derived sulfur abundances due to possible uncertainties on the stellar atmospheric parameters. Table 3 presents the mean variations of [S/H] when considering typical AMBRE uncertainties (external errors estimated by comparison with external catalogues) on $T_{\rm eff}$, log(g), and [M/H] for the different stellar types contained in our sample. We note that typical uncertainties on the microturbulence velocity (±1 km s^{-1}) and [α/Fe] (±0.1 dex) have no measurable effect on [S/H]. It can be seen that the sulfur abundances are mostly sensitive to the $T_{\rm eff}$ uncertainties, and this effect is stronger for the coolest stars in which sulfur lines are weaker. The reported total uncertainties on the sulfur abundances have been estimated by summing quadratically the different contributions.

Then, since we were able to analyse several spectra of the same stars (repeats) spanning a wide range of S/N, we checked the robustness of our automatic procedure for deriving sulfur abundances. The AMBRE large sample of repeat spectra allowed us to precisely quantify our typical internal uncertainties that could result from several effects (e.g., continuum normalisation, spectra quality, radial velocity correction, differences in the atmospheric parameters). We list in Table 4 the internal errors for different stellar types. For a given line and a given stellar type it can be seen that the sulfur abundance scatter from spectra to spectra is already very small at rather low S/N, and can even be smaller for higher S/N. The robustness of our automatic procedure is therefore confirmed. Moreover, we note that our final sulfur abundances are computed by averaging the repeated measurements and up to three sulfur lines, when available. Consequently, the relative uncertainties from star to star in the AMBRE-sulfur catalogue are therefore even smaller than the values given in Table 4. In any case, they can be neglected with respect to other error sources as errors caused by possible atmospheric parameter uncertainties similar to those reported in Table 3.

3. AMBRE catalogue of sulfur abundances

The final AMBRE catalogue of mean sulfur abundances is reported in Table 5; a full version is available in electronic form. Having applied all the rejection criteria of Sect. 2.3.2 (repeat spectra with departing stellar parameters, high-rotating stars, too low S/N spectra and non-detected lines) and the above averaging procedures, we finally provide the sulfur abundances with the associated dispersion for 1,855 different stars. Among them, about 10% are giant stars and the studied metallicity domain varies from ~ −1.9 dex to ~+0.7 dex. These numbers have to be compared to the 719 stars with sulfur abundance of CS20 and to the 1301 sulfur abundances of Duffau et al. (2017). The AMBRE-sulfur catalogue is therefore the largest ever published. Moreover, it covers a metallicity range larger than any other, particularly in the metal-poor regime since almost 30 stars have [M/H] < −1.0 dex.

In Table 5 the stars are identified by their *Gaia* DR2 ID, except for six that only have a HD name. This table contains the mean atmospheric parameters ($T_{\rm eff}$, log(g), [M/H], [α/Fe]) together with the mean S/N[1] of the spectra kept when computing the mean final sulfur abundances. We recall that these parameters were averaged by adopting exactly the same WM procedure as for the abundances (see previous section). For a given star we also provide the number of analysed sulfur lines for each component of multiplet 8 (N_{6743}, N_{6748}, N_{6757}) that have finally been considered when computing its sulfur abundance. These numbers range from unity (only one spectrum available) to several thousands when a large number of repeat spectra were kept. The largest numbers of individual abundances derived for a given star are 5194, 4616, and 5636 for the three sulfur components, respectively. We also report 1165, 1426, and 1855 stars with at least one measurement of the 674.3, 674.8, and 675.7 nm line, respectively. Moreover, 1049 stars have the three sulfur lines

[1] Estimated with the AMBRE pipeline during the parametrisation process, i.e., at a spectral resolution $R \sim 15\,000$.

Table 5. AMBRE catalogue of LTE sulfur abundances.

Star ID [(a)]	S/N	$T_{\rm eff}$(K)	log(g)	[M/H]	[α/Fe]	N_{6743}	N_{6748}	N_{6757}	[S/H]	$\sigma_{\rm [S/H]}$
105332908999068032	68	5711	4.42	0.30	−0.02	0	2	1	0.31	0.01
1153682508388170112	26	6100	4.11	−0.08	0.01	9	16	20	0.05	0.04
1155587858959873024	290	5795	4.04	−0.83	0.27	0	2	1	−0.55	0.07
1160260989536170880	220	5743	4.35	0.02	−0.05	0	1	4	0.07	0.01
1160956465000504448	62	5426	4.55	0.04	0.03	0	1	2	−0.01	0.11
1167602394315412864	94	5619	3.69	−0.95	0.33	6	12	17	−0.56	0.03
1174143182830505984	69	5744	4.68	0.17	0.06	0	1	1	0.10	0.07
...	...	...	...	...	...	...	...	...	...	...
...	...	...	...	...	...	...	...	...	...	...

Notes. The full electronic table is available at the CDS. [(a)]*Gaia* DR2 ID except HD-name for six very bright stars not present in the *Gaia* second data release.

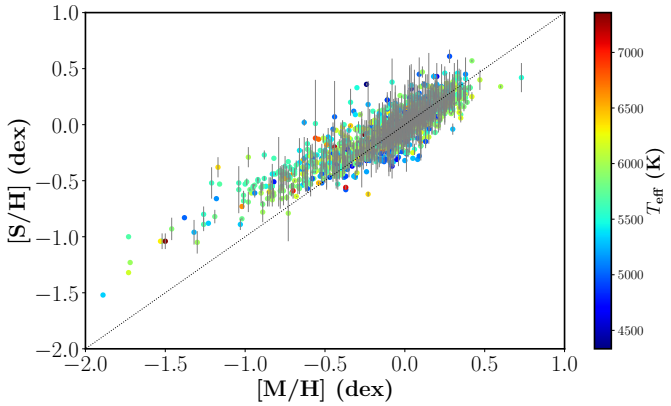

Fig. 1. AMBRE-sulfur abundances [S/H] as a function of the mean stellar metallicity [M/H] for the whole sample. Error bars are the line-to-line dispersions listed in Table 5. The stars without error bars are those with only one measured sulfur line (the 675.7 nm transition), hence no line-to-line scatter can be estimated.

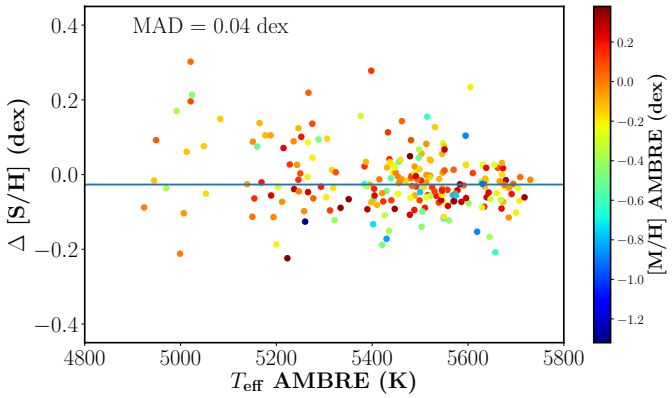

Fig. 2. Comparison between the AMBRE and Costa Silva et al. (2020) sulfur abundances. The ordinate axis refers to the difference ([S/H]$_{\rm AMBRE}$ − [S/H]$_{\rm literature}$). The blue horizontal line indicates the median of these differences (−0.027 dex), and the associated median absolute deviation is shown in the upper left corner. This MAD is equal to 0.03 dex if we only consider stars warmer than 5400 K (see text).

measured in at least one of their spectra. Finally, as an indicator of the measurement uncertainty, we also report the dispersion ($\sigma_{\rm [S/H]}$) between the different measurements obtained for a given star (equivalent to a line-to-line scatter between lines and/or repeats). We note that this scatter can differ from the individual line error Δ[S/H] described in the previous section. The mean of these scatters is equal to 0.06 dex, and a dispersion lower than 0.02 and 0.05 dex is found for 29% and 57% of the sample stars, respectively. We can therefore safely conclude that the reported sulfur abundances are very precise and consistent with each other. The derived sulfur abundances are shown in Fig. 1 as a function of the mean stellar metallicity. For positive metallicities it can be seen that the sulfur abundances behave, in a first approximation, almost as [M/H]. However, [S/H] becomes increasingly higher than [M/H] for negative metallicities down to [M/H] ∼ −1.0 dex, after which [S/H] − [M/H] stays almost constant down to [M/H] ∼ −2.0 dex. This behaviour is very similar to that of the α-elements, suggesting that sulfur belongs to this class of chemical species (see discussion in Sect. 4.1).

As a quality check of our derived sulfur abundances, we first verified that no systematic trends are present between the AMBRE [S/H] and the effective temperature (over the range 4500–6500 K) or the surface gravity (which varies between 1.5 and 5.0 cm s^{-2}). We also compared our complete sample of sulfur abundances (i.e., without selecting the best ones as done below) with those of CS20 estimated from the HARPS spectra of solar-type stars (see Fig. 2). This catalogue contains a very large number of stars (223) in common with ours. This large number is explained by the fact that both samples contain several HARPS spectra collected over similar epochs (most of them probably identical spectra). The median of the differences between the literature and the AMBRE values of [S/H] is insignificant (−0.027 dex) with a very small associated dispersion, the MAD and the standard deviation being equal to 0.04 dex and 0.08 dex respectively (see Fig. 2). We note that a large part of these small differences can be explained by the different atmospheric parameters adopted in the two studies. For example, the dispersion associated with the differences in $T_{\rm eff}$, log(g), and [M/H] are 63 K, 0.14, and 0.05 dex, respectively. It can be seen, however, that the differences in [S/H] seem to slightly increase towards cooler stars, revealing perhaps some differences in the analysis (possibly caused by different considerations of some molecular blends?). Moreover, CS20 seem to favour in their discussion their stars with effective temperatures within ±500 K around the solar value, the range in which their errors are smaller. For the stars in common and having $T_{\rm eff} \geq 5400$ K, the agreement is indeed better since the MAD and the standard deviation decrease to 0.03 dex and 0.06 dex, respectively (the median of the differences staying insignificant). As a consequence, we can safely conclude that the agreement between the two independent analyses is very satisfactory, and this confirms the high accuracy of the AMBRE catalogue of automatically derived sulfur abundances.

Table 6. AMBRE LTE sulfur abundances of the *Gaia* benchmarks stars adopting their recommended atmospheric parameters.

Star	*Gaia* DR2 or HD	S/N	$T_{\rm eff}$(K)	log(g)	[M/H]	[α/Fe]	N_{6743}	N_{6748}	N_{6757}	[S/H]	$\sigma_{\rm [S/H]}$
Solar-type stars											
α Cen B	HD128621	45	5231	4.53	0.22	0.04	39	239	1013	0.25	0.25
τ Cet	2452378776434276992	89	5414	4.49	−0.49	0.23	615	1406	2505	−0.38	0.03
Sun/Vesta	–	>1000	5771	4.44	0.00	0.00	1	1	1	0.00	–
α Cen A	HD128620	80	5792	4.31	0.26	−0.02	11	12	17	0.17	0.01
18 Sco	4345775217221821312	79	5810	4.44	0.03	0.02	1854	1863	2281	0.00	0.04
HD 22879	3250489115708824064	124	5868	4.27	−0.86	0.33	12	17	20	−0.57	0.01
μ Ara	5945941905576552064	62	5902	4.30	0.35	0.00	626	1482	2849	0.14	0.02
FGK subgiants											
δ Eri	5164120762332790528	76	4954	3.76	0.06	0.04	0	18	275	0.12	0.07
β Hyi	4683897617108299136	102	5873	3.98	−0.04	−0.02	2601	1162	2762	−0.17	0.01
β Vir	3796442680947600768	89	6083	4.10	0.24	−0.13	236	204	249	0.12	0.01
F dwarfs											
Procyon	HD61421	128	6554	4.00	0.01	−0.04	2662	4844	5681	0.00	0.01
HD 49933	3113219383954556416	105	6635	4.20	−0.41	0.04	300	164	470	−0.49	0.03
Cool giant											
ϵ Vir	3736865265439463424	64	4983	2.77	0.15	−0.07	0	2	5	0.12	0.04

Notes. The electronic table is available at the CDS.

Finally, we provide in Table 6 new sulfur abundance of the *Gaia* benchmark stars present in our sample (several of them having a very large number of available spectra). These FGK-type stars have carefully studied atmospheric parameters derived using different analysis techniques, and they are thus very helpful to calibrate and/or validate large spectroscopic surveys. Although these stars are already present in Table 5, their AMBRE atmospheric parameters may differ slightly from the commonly accepted values. We therefore recomputed their sulfur abundances from all their available spectra, assuming for each of them the accepted parameters summarised in Jofré et al. (2018) (where the adopted [α/Fe] is the mean of the individual Mg, Si, Ca, and Ti abundances). We note that, for the Sun, we analysed a very high-S/N HARPS spectrum of Vesta. These new [S/H] values in Table 6 differ only marginally (by a few hundredths of dex) from those of Table 5 and this only results from the small differences in the adopted atmospheric parameters. These new abundances should be favoured in any future calibration or validation studies of sulfur abundances.

4. Behaviour and evolution of sulfur in the Milky Way

In this section we analyse the catalogue presented above by selecting stars with the best measured sulfur abundances. For this purpose we use the following:

– For [M/H] ≥ -1.0 dex: We selected stars having a sulfur abundance dispersion $\sigma_{\rm [S/H]}$ lower than 0.05 dex (i.e., those having at least two lines measured consistently).

– In the same metallicity regime: We kept the other stars having only the 675.7 nm component, but measured in a high-quality spectrum ($S/N > 100$).

– For the metal-poor regime ([M/H] < -1.0 dex): Because fewer stars are available, we slightly relaxed these strict criteria by adding any stars having spectra with S/N higher than 50.

The resulting subsample consists of 1203 stars with very high-quality sulfur abundances (65% of the whole AMBRE-sulfur catalogue, see top panel of Fig. 3).

We also built a golden sample by selecting stars with even better sulfur abundances and satisfying the following criteria:

– They should have at least three measurements of each individual SI line (i.e., with at least nine abundances available to estimate their mean sulfur abundance) and a total dispersion $\sigma_{\rm [S/H]}$ lower than 0.05 dex for their mean [S/H].

– We also included metal-poor stars ([M/H] < -1.0 dex) having fewer measured lines, but spectra with a S/N higher than 150.

This golden sample contains 540 stars with extremely high-quality and precise sulfur abundances. They are shown in the three bottom panels of Fig. 3. The properties of these best stars are described in more detail below, but the same conclusions are reached with the largest sample of 1,203 stars, although the slightly larger dispersion could slightly blur some of the figures shown in the following. Finally, we discuss the sulfur abundances with respect to the mean metallicity ([S/M]) obtained by substracting the [S/H] estimated in the present work from the mean metallicity [M/H] previously derived within the AMBRE Project ([Fe/H] abundances estimated from individual iron lines being not available for the whole sample).

4.1. Sulfur as an α-element

Because of its nucleosynthesis channel, sulfur belongs to the family of the α-elements, as do oxygen and magnesium, for example. For these chemical species Milky Way evolution models predict a specific variation of the abundance ratio of α-elements to iron ([α/Fe]) with respect to metallicity [M/H]. This is observationally confirmed for most α-species, including sulfur to a lesser extent (see the Introduction for references). However, the present AMBRE-sulfur catalogue offers the possibility to draw a more global and homogeneous picture of the sulfur abundance variations in the Milky Way than the previous studies, thanks to its large statistics, accurate measurements, and large metallicity range covered.

As already shown in Fig. 1 for the complete sample, and more clearly shown in Fig. 3 for the high-precision and golden samples exhibiting our very best sulfur abundances, the abundance ratio of sulfur to mean metallicity ([S/M]) exhibits a variation with respect to the mean metallicity that is very similar to

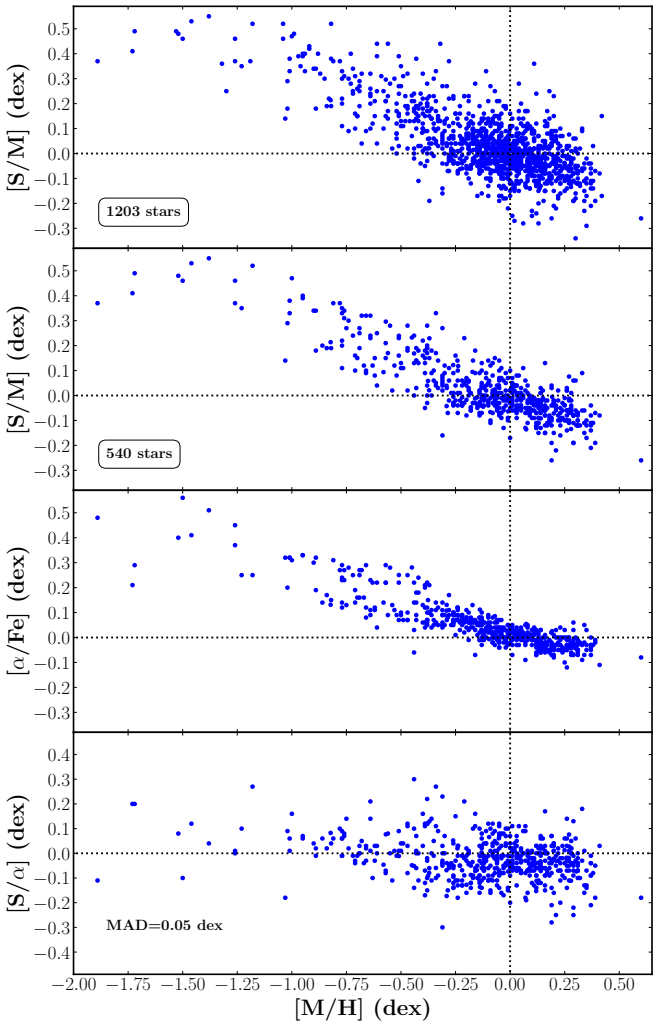

Fig. 3. Ratio of sulfur abundance to mean metallicity [S/M] as a function of the mean stellar metallicity [M/H] for the best derived abundances. *Top two panels*: dispersion smaller than 0.05 dex and/or high-S/N spectra (*top panel*) and the same criteria plus a selection of stars having at least three measurements of the three individual SI lines (golden sample, second panel from top). *Bottom two panels*: behaviour of [α/Fe] and [S/α] vs. mean metallicity for the golden sample.

that of the mean [α/Fe] ratio provided by the AMBRE Project (third panel of Fig. 3). The dispersion is smaller for [α/Fe] because it is derived from a much larger number of lines belonging to different chemical species than the maximum of three sulfur lines studied in this work. This similar behaviour between sulfur and α-elements is also clearly illustrated in the bottom panel of Fig. 3 where the mean [S/α] value is equal to zero with a very small dispersion over the whole metallicity range (MAD = 0.05 dex).

On the other hand, the suspected plateau (see Introduction) of the metal-poor regime (Galactic halo stars with [M/H] $\lesssim -1.0$ dex) can be studied thanks to the 27 stars analysed in this work (only those of the golden sample are shown in Fig. 3). This number of stars is much larger than the numbers reported by other large surveys of sulfur abundances (only two stars in CS20 and about half a dozen in Duffau et al. 2017). It should be noted that the mean [S/M] in the metal-poor regime is found at +0.44 dex, a classical level for α-elements. The variation of [S/M] with metallicity for [M/H] $\lesssim -1.0$ dex is compatible with a flat behaviour, as confirmed by a locally weighted scatterplot smoothing (LOWESS) fit of the data (Cleveland 1979). However, a rather large dispersion (close to 0.15 dex) around this mean can be seen, probably caused by the difficulty in measuring the sulfur lines in this low-metallicity domain in spectra with S/N that can be as low as 50 for the high-precision sample. Nevertheless, our study therefore invalidates the suggestion of a steady increase in [S/M] with decreasing metallicities (see discussion in the Introduction). However, the ratio [S/α] seems to become slightly positive (although with a large dispersion; see Fig. 3 bottom panel) for these low metallicities: the mean [S/α] for [M/H] $\lesssim -1.0$ dex is close to 0.07 dex with a dispersion MAD = 0.065 dex. This dispersion could result from the analysis, but it could also reflect the fact that the lines of different chemical species adopted to derive the α-abundances could differ from one metallicity regime to another. As a consequence [α/Fe] could more or less correlate with [Mg/Fe], for example, depending on [M/H]. We note, however, that the dispersion in [α/Fe] looks larger than in [S/M] in this low-metallicity regime. Such a dispersion could therefore reveal the heterogeneity nature of the Galactic halo.

We now focus on the supersolar metallicity regime ([M/H] $\gtrsim 0$) where the values of [S/M] and [α/Fe] shown in Fig. 3 become negative. This decrease is extensively discussed in Santos-Peral et al. (2020a) for magnesium and, independently, clearly seen again here for sulfur. This continuous decrease is not seen in the sulfur sample of CS20, and not always seen in other Galactic studies of [α/Fe] behaviours. We recall that Santos-Peral et al. (2020a) show that the flattening reported by some previous studies is an artefact created by an incorrect continuum normalisation procedure in crowded-line spectra of very metal-rich stars. We also note that this decrease for sulfur and magnesium is in perfect agreement with Galactic evolution models. There is no reason why the production rate of α-elements (and sulfur) would suddenly increase around solar metallicity and/or why the iron production would be constant or smaller to produce an almost constant [α/Fe] ratio at high metallicity. For instance, Palla et al. (2020) predict an [α/Fe] ~ -0.2 dex at [M/H] $\sim +0.5$ dex in close agreement with our observations (see also the models of Prantzos et al. 2018; Romano et al. 2010; Kobayashi et al. 2020).

Then, we compared the AMBRE-sulfur abundances with magnesium abundances previously derived within the AMBRE Project. We first show in Fig. 4 stars having accurate Mg abundances derived in Santos-Peral et al. (2020a) from carefully selected lines and for which the normalisation procedure was optimised for the high-metallicity regime. To increase the size of the comparison sample, we slightly relaxed the quality criterion of the selected sulfur abundances (dispersion lower than 0.1 dex) and this resulted in 89 stars in common between both catalogues. Again, the two α-elements Mg and S show the same overall behaviour with metallicity. The median [S/Mg] ratio over the whole metallicity range is close to -0.05 dex with an extremely small dispersion (MAD = 0.03 dex). This median is close to -0.08 dex and -0.03 dex for [M/H] < -0.25 dex and [M/H] > -0.1 dex (with similar small dispersions), respectively. We also note that, for these metallicity regimes, the median of [α/Mg] is equal to -0.05 dex and 0.0 dex, respectively, leading to the slightly negative mean [S/α] ratio shown in Fig. 3 when [M/H] $\gg -1.0$ dex. Such [S/Mg] ratios could be caused by different calibrations adopted for the abundance derivations (although the procedures adopted by these studies are very similar), but could also be real since the production rates (yields) of these two elements could be slightly different. Our slightly

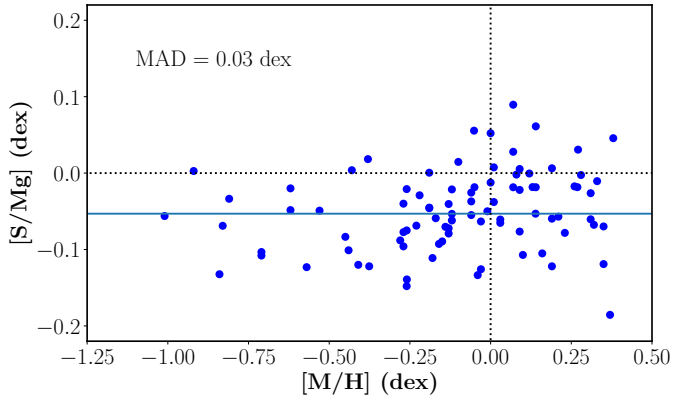

Fig. 4. Ratio of sulfur to magnesium abundance [S/Mg] as a function of the mean stellar metallicity [M/H] for stars in common with Santos-Peral et al. (2020a). The blue horizontal line indicates the median of [S/Mg] (−0.05 dex) over the whole metallicity domain and the associated median absolute deviation is reported in the upper left corner.

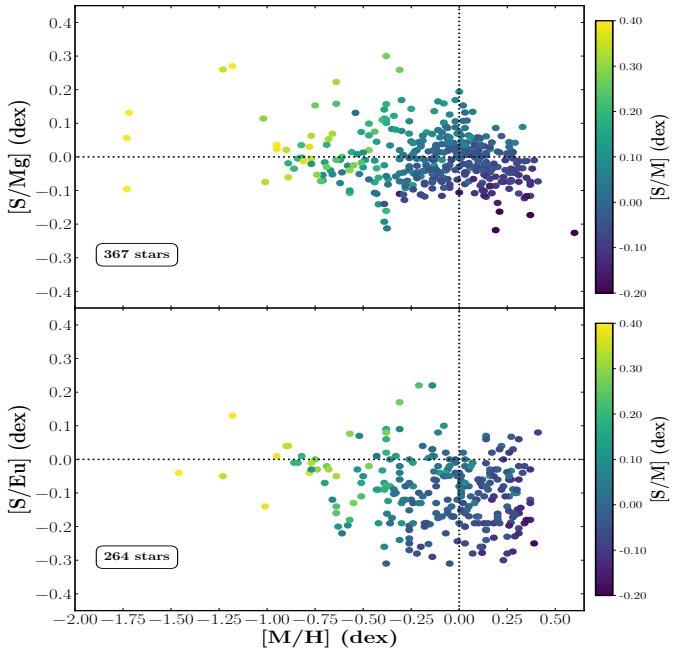

Fig. 5. Abundance ratios of sulfur to magnesium ([S/Mg], *top panel*) and to europium ([S/Eu], *bottom panel*) as a function of the mean stellar metallicity [M/H] colour-coded with [S/M], adopting Mg and Eu abundances derived by Mikolaitis et al. (2017, *top panel*) and Guiglion et al. (2018, *bottom panel*).

negative [S/Mg] ratio in the metal-poor regime seems to differ from the positive [S/Mg] value predicted by Kobayashi et al. (2020, Fig. 5) and Prantzos et al. (2018, Fig. 13), whereas the agreement seems much better for metal-rich stars. Finally, the variation of [S/Mg] with metallicity (higher at higher [M/H]) could suggest that these two elements do not vary in perfect lockstep during the whole Galactic evolution (but see Fig. 7, middle panel).

We compare in the top panel of Fig. 5 the sulfur-to-magnesium abundance ratio with respect to the metallicity adopting the magnesium abundances from the study of Mikolaitis et al. (2017). We considered the best derived magnesium abundances of this work by rejecting those with too large errors, and found 367 stars in common. We also show in the bottom panel of Fig. 5 a similar plot showing the sulfur-to-europium abundance ratio thanks to data derived by Guiglion et al. (2018). Here, we selected the best Eu abundances derived from at least two lines and having a small dispersion (264 stars are found in common with the AMBRE-sulfur sample). From these two plots it can be seen that sulfur, magnesium, and europium are closely correlated and follow a similar behaviour: the abundance ratios seem to be rather constant with the metallicity. More precisely, the top panel of Fig. 5 is very similar to Fig. 4, although the dispersion is larger, probably resulting from the different methodoloy adopted by Mikolaitis et al. (2017) for deriving Mg abundances. Regarding the [S/Eu] ratio, it also seems to stay constant with metallicity, although sulfur could be slightly underabundant (by about ∼0.15 dex) with respect to europium at any metallicity. Thus, since magnesium and europium are believed to be predominantly produced in Type II supernovae (although other production sites are invoked for Eu), Fig. 5 again confirms that sulfur could be predominantly produced by the same nucelosynthesis channel in SN II.

In summary, and as a conclusion of this subsection, we can therefore safely state that the α nature of sulfur is clearly confirmed by the AMBRE Project over a very large metallicity domain.

4.2. Kinematic and orbital properties

Thanks to *Gaia*/DR2 astrometry (Gaia Collaboration 2018) and associated distances from Bailer-Jones et al. (2018), we computed the Galactic cartesian coordinates of our sample stars. As expected, our sample is predominantly composed of stars located in the solar vicinity: about 90% of them are found within 200 pc of the Sun. Moreover, except for a few cases that are found at a distance from the Galactic plane up to ∼1 kpc, most stars are located within a distance smaller than 400 pc from the plane. Their kinematic properties were then estimated thanks to the AMBRE radial velocities, assuming that the Sun is located in the Galactic plane at 8.2 kpc from the centre and adopting the velocities reported by Schönrich et al. (2010) for its motion with respect to the local standard of rest. Finally, orbital parameters were calculated with the *galpy* code Bovy (2015). We refer to Santos-Peral et al. (2021) for a detailed description of the methodology adopted for computing these orbits.

The complex chemo-dynamical characteristics of the disc stellar populations are still a matter of debate, and are constantly being updated thanks to progressively more complete samples inside and outside the solar neighbourhood. It is today largely admitted that the Galactic disc presents a chemo-dynamical bimodality, usualy described as the combination of two components: the thin and the thick disc. Since the discovery of this bimodality in stellar density distributions (Yoshii 1982; Gilmore & Reid 1983) several studies have shown the kinematical (e.g., Bensby et al. 2003; Reddy et al. 2006; Kordopatis et al. 2017) and chemical (e.g., Adibekyan et al. 2012; Recio-Blanco et al. 2014; Hayden et al. 2015) distinctions between the two components. The thick-disc presents a larger scale height and a shorter scale length, and it is kinematically hotter with respect to the thin-disc. It is also reported to be [α/Fe] enhanced with respect to the thin disc at all metallicities. Finally, the stellar age distribution is older for the thick disc than for the thin disc. Different evolution models and simulations have tried to interpret the observed distributions. Although the Galactic disc evolution is still a matter of debate, it is generally accepted that the thick disc phase corresponds to the early

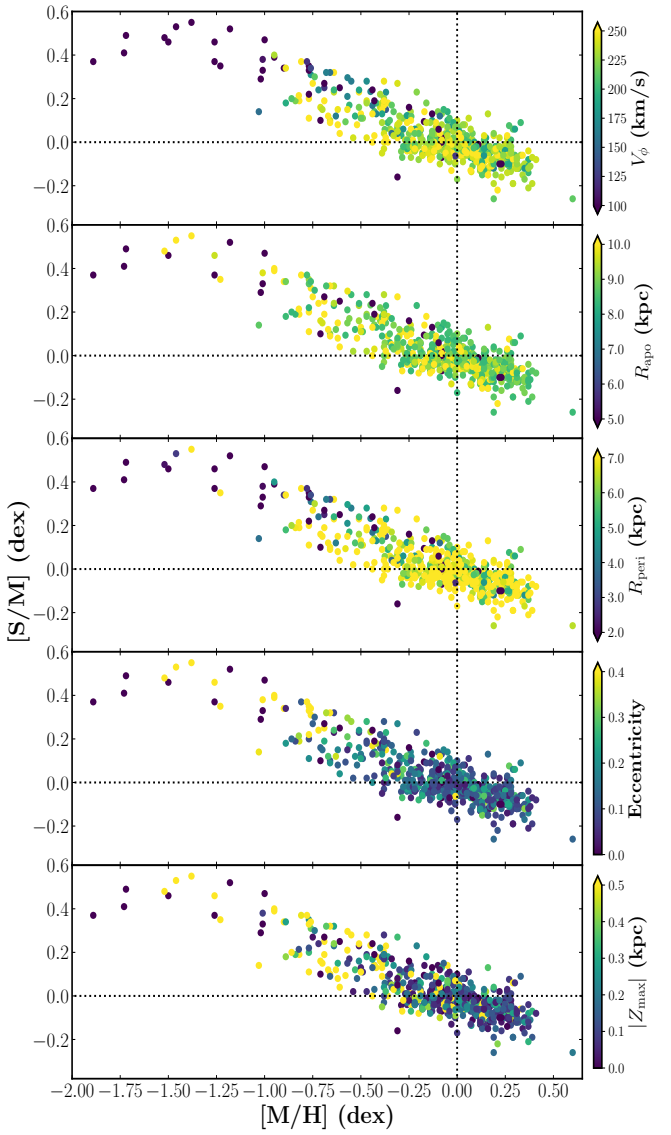

Fig. 6. Ratio of sulfur to mean metallicity [S/M] as a function of the mean metallicity [M/H] colour-coded (*from top to bottom*) by the rotational velocity (V_ϕ), the pericentre and apocentre radii (R_{peri} and R_{apo}), the eccentricity, and the maximum height above the Galactic plane (Z_{max}).

disc component, and that about 8 Gyr ago a discontinuity in the disc evolution allowed the formation of the thin disc. The study of the disc dichotomy using sulfur abundances has been hindered until now by the lack of good statistics and the low precision of the abundance estimates. In this section we take advantage of our large sample of precise sulfur abundances in the solar neighbourhood to analyse the chemo-dynamical correlations in the [S/M] versus [M/H] plane.

We show in Fig. 6 how the sulfur abundances of the best sample defined earlier (golden sample, see Fig. 3) are related to some of their stellar orbital properties such as the pericentre and apocentre radii (R_{peri} and R_{apo}), the eccentricity (e), the rotational velocity (V_ϕ), and the maximum height above the Galactic plane (Z_{max}).

First, a gap can be suspected between the [S/M]-rich and the [S/M]-poor populations, although its precise location cannot be easily defined, as is often the case for the other α-elements. We note, however, that the chemical separation of the two disc components seems to depend on the studied α-element (see e.g., Mikolaitis et al. 2017). Nevertheless, the kinematical and dynamical characterisation confirms that the observed [S/M] dispersion at a given metallicity is not the result of the abundance uncertainties, clearly illustrating the above-described disc bimodality. This is particularly true for stars having metallicities lower than −0.5 dex. As is the case for other α-species, the thick versus thin disc dichotomy is observed to be blurred at higher metallicities, and is today a matter of debate (Adibekyan et al. 2012; Hayden et al. 2017).

More specifically, it can be clearly seen in Fig. 6 that metal-poor sulfur-rich stars (MPSR, for metallicities found between $[-1.0, -0.5]$) have orbital properties that strongly differ from the more metal-rich sulfur-poor ones (MRSP):

– First, regarding the rotational velocity, two disc components are present and they differ in V_ϕ and [S/M]. The less enriched sulfur stars (thin disc) have lower rotational velocities close to the solar velocity. Only the most metal-poor stars have much lower rotational velocities. A gradient of V_ϕ with [M/H] is also seen, as already mentioned for other α-species (see e.g., Recio-Blanco et al. 2014; Kordopatis et al. 2017).

– Then, most of the MPSR are found in the inner Galactic regions contrarily to the MRSP that are predominantly located close to the solar apocentrer and pericentrer radii. Radial gradients in both R_{peri} and R_{apo} can also be suspected (for a given metallicity bin), and they are correlated with the [S/M] enrichment. For instance, at a given metallicity (for [M/H] $\gtrsim -1.0$ dex), stars having a smaller apocentre radius are the most enriched in sulfur (for a similar discussion, see Hayden et al. 2017). If thick-disc stars are defined as being more sulfur-rich (see Sect. 4.4), it can be easily seen that the thick disc is more radially concentrated than the thin disc.

– The eccentricity of the MPSR is higher than the that of the MRSP, and every star with a metallicity higher than ~ -1.0 dex is on a quasi-circular orbit ($e \lesssim 0.15$). Only the most metal-poor stars with the highest [S/M] ratios are found on eccentric orbits, as is the case for halo stars, with a few exceptions (also detected in Z_{max}) confirming the wide range of stellar orbits in this metallicity range.

– Finally, the bottom panel of Fig. 6 reveals a settling of the disc stars for the MRSP, and the MPSR are mostly found at several hundreds of parsecs above the Galactic plane, as already described in Hayden et al. (2017).

In summary, Fig. 6 shows that the two disc components can be defined by studying both the kinematic and the sulfur content. This confirms the high quality of the sulfur abundances of the selected stars, and we show in Sect. 4.4 that the thin and thick disc could also be defined based solely on their sulfur content, as could be done by adopting any other α-elements.

Furthermore, Fig. 6 also reveals that all the metal-poor ([M/H] $\lesssim -1.0$ dex) stars of the sample have much lower rotational velocities than the more metal-rich stars. These V_ϕ values lower than $\sim$150 km s^{-1} are typical of halo star members. However, it can also be seen in the bottom panel of Fig. 6 that a large part of them are located very close to the Galactic plane. This could reveal that these halo stars are presently crossing the plane. Their large number could result from the complex selection function of the AMBRE catalogue revealing a possible bias towards the identification of metal-poor stars in the solar neighbourhood.

4.3. Sulfur abundances and stellar ages

Santos-Peral et al. (2020b) have estimated accurate and reliable ages for about 400 AMBRE stars using an isochrone fitting method, as in Kordopatis et al. (2016), and distances from

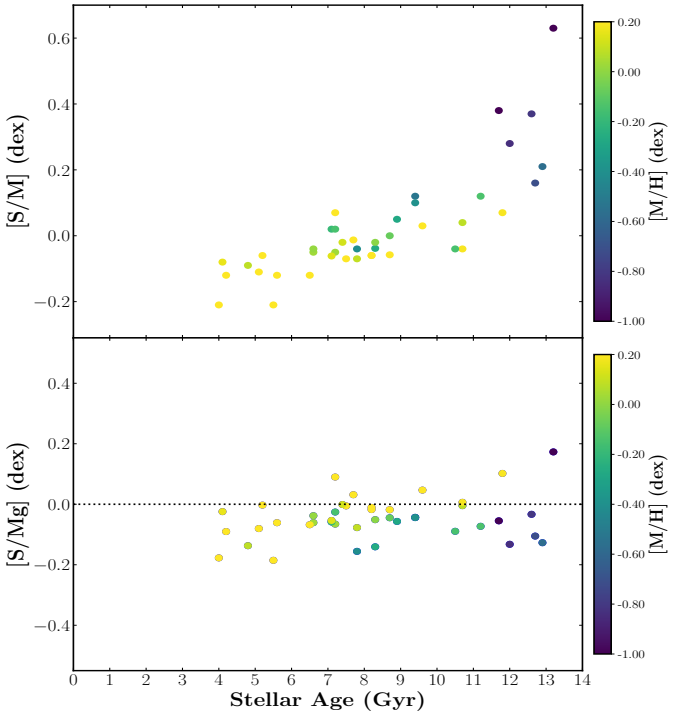

Fig. 7. Ratio of sulfur abundance to mean metallicity [S/M] (*top panel*) and to magnesium abundance [S/Mg] (*bottom panel*) as a function of the stellar ages for the main sequence turn-off and subgiant stars of the sample. The colour-coding corresponds to the mean stellar metallicity.

Bailer-Jones et al. (2018, based on *Gaia*/DR2 parallaxes). For this purpose they selected only main sequence turn-off and subgiant stars for which age estimates are more accurate since stellar ages increase quickly when stars cross these regions of the HR-diagram. We refer to this article for a detailed description of the adopted methodology to derive the stellar ages adopted in the present study.

Among our golden sample of stars with the best derived sulfur abundances, about 10% are in common with Santos-Peral et al. (2021) and have ages with rather small uncertainties (the mean of their age relative errors is equal to 17% with a dispersion of 9%). The variation of [S/M] and [S/Mg] abundance ratios as a function of the stellar ages and colour-coded with the mean metallicity are shown in Fig. 7. The following can be seen:

– The [S/M] ratio (top panel) of disc stars decreases towards younger and more metal-rich stars in a continuous way from ∼10 Gyr to ∼4 Gyr and with a rather small dispersion. Moreover, this decrease is also seen down to negative [S/M] values for ages younger than ∼5–6 Gyr. We clearly see the sulfur depletion with respect to iron in the solar vicinity for the youngest stars. We found a slope for the [S/M] versus age relation close to $\sim 0.02\,\mathrm{dex\,Gyr^{-1}}$ for stars younger than ∼10 Gyr (in very good agreement with the gradient reported by Santos-Peral et al. 2020b, for magnesium). This contradicts some previous claims where most thin-disc stars seem to have almost constant [S/M] ratios with age; for instance, the slope in CS20 is two times smaller. However, the behaviour shown in Fig. 7 is easy to interpret: As expected by chemical evolution models, the [α/Fe] content of stars in the supersolar metallicity regime is believed to continue to decrease with time (the production of α-species by SNII is strongly reduced with respect to that of iron-peak elements in SNIa). More explicitly, younger metal-rich stars should always have lower [α/Fe] (and hence [S/M]) ratios, as predicted by any chemical evolution model of the Galactic discs (for a recent reference, see Fig. 9 in Palla et al. 2020).

– The stars older than ∼8 Gyr follow the same behaviour as younger stars: the older they are, the more sulfur-enriched and metal-poor they are. However, the increase in [S/M] with age is much faster and steeper. Moreover, all the oldest stars in our sample, which are the most metal-poor, are enriched in sulfur. Once again, this is in complete agreement with chemical model predictions.

– It can also be seen in the bottom panel of Fig. 7 that sulfur and magnesium abundances stay close to each other whatever the stellar age (but see the above discussion on this [S/Mg] ratio at different metallicities). This could reveal that there is no important variation in the yields of these two species with time, and could again confirm their common origin in SNII explosion.

As a conclusion of the present subsection, it can be said that sulfur can be considered a good chemical clock, like any other α-species, although some dispersion may be present (see e.g., Santos-Peral et al. 2020b).

4.4. Sulfur in the different Galactic populations

A dichotomy in the [α/Fe] abundances, associated with the thin disc–thick disc bimodality, has been found in the Galactic disc stellar populations (see e.g., Adibekyan et al. 2011; Recio-Blanco et al. 2014). To date, such a chemical separation has been found either using an averaged [α/Fe] index (see above references), but also using different individual α-species such as magnesium (e.g., within the AMBRE context Mikolaitis et al. 2017; Santos-Peral et al. 2020a) or other individual [α/Fe] ratios (Mikolaitis et al. 2014, among others). However, such a chemical dichotomy has never been established using only sulfur abundances. We note that in the very recent study of CS20 the thin–thick disc separation was first defined thanks to a global [α/Fe] abundance ratios and then applied to and/or checked against their sulfur content. We decided to follow an opposite approach by looking for a possible definition of the Galactic components based purely on their sulfur abundances. We indeed recall that, as already mentioned in Sect. 4.2, the dichotomy of the two disc components is clearly seen in kinematics and is correlated to the sulfur content. This approach is also favoured since the thin–thick disc separation is expected to slightly differ from one α-species to another, as already shown by Mikolaitis et al. (2014) or more recently by Amarsi et al. (2020). Such different behaviours for different α-elements could be real (slightly different nucleosynthesis channels) or caused by (among other possibilities) different internal dispersions resulting from different residual systematics such as non-LTE effects and/or different sensibilities of the selected lines between dwarfs and giants (the proportion of dwarfs and giants in either disc being different due to observational selection functions).

Defining the sulfur-rich/sulfur-poor separation (associated hereafter with the α-rich/α-poor or thick-disc/thin-disc Galactic populations, respectively) could be useful, among other interests, to compute the radial chemical gradients in both discs. For this purpose we first selected our best sulfur abundances by keeping only stars having a large number of analysed spectra. More specifically, we considered 200 stars having more than 20 independent measurements of their 675.7 nm line, more than 50 analysed lines in total including at least three measurements of the three SI lines, and, in addition, an internal dispersion among all these measurements smaller than 0.05 dex. These best measured stars are shown in the top panel of Fig. 8. We also defined a separation to disentangle the thin and thick discs

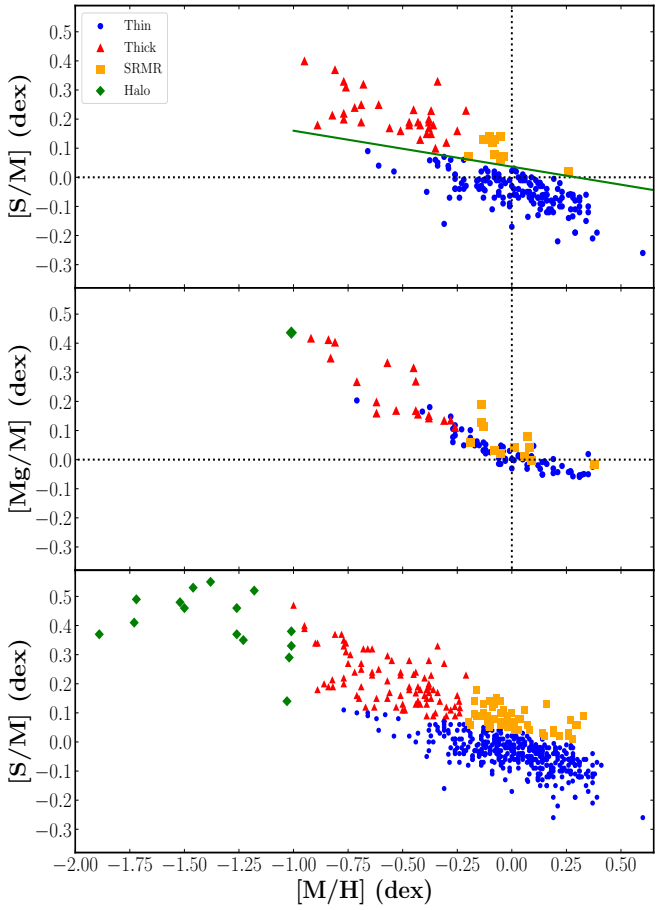

Fig. 8. *Top*: ratio of sulfur abundance to mean metallicity [S/M] vs. mean metallicity [M/H] for stars with the best measured sulfur abundances (large number of analysed spectra, at least three measurements of the three SI lines available and small dispersion). The green line shows the adopted separation between the sulfur-rich and sulfur-poor stars. *Middle*: [Mg/M] ratio vs. [M/H] for the stars in common with Santos-Peral et al. (2020a). *Bottom*: same as top panel, but for the complete sample of 540 stars with the best derived abundances (same sample as in Fig. 3, second panel), and labelled according to their Galactic population membership. In all these panels thin-disc, thick-disc, sulfur-rich, metal-rich, and halo stars are shown as blue filled circles, red triangles, orange squares, and green diamonds, respectively.

(green line in Fig. 8). It was drawn by examinating the [S/M] distributions in 0.2 dex wide metallicity bins for [M/H] varying within $[-1.0, 0.0]$. Then, we looked for the position of the low-density regions separating both disc sequences, and drew a straight line along these minima. This green line was then extrapolated towards supersolar metallicites. Then, this separation was applied to both the entire and the golden samples. The resulting ∼65% sulfur-poor, thin-disc stars are shown as blue filled circles below the green line in the bottom panel of Fig. 8. Moreover, for the sulfur-rich stars (found above the separation line), a gap in their number distribution might be present around [M/H] = −0.2 dex. Such a gap was already suspected among α-rich stars around the same metallicity by Adibekyan et al. (2011), who proposed to call them high-α metal-rich stars (see also Gazzano et al. 2013). Although not clearly seen in sulfur and sometimes absent in other studies of α elements, depending on the analysed sample, we nevertheless decided to label such stars separately. This led to ∼18% sulfur-rich metal-rich stars (hereafter SRMR, and shown as orange squares in Fig. 8) and ∼15% thick-disc stars as red triangles. Finally, the stars more metal-poor than −1.0 dex were labelled as potential Galactic halo members (green diamonds).

In confirmation of the above, several remarks can be made regarding the bottom panel of Fig. 8. First, it can be again seen that the sulfur abundances of the thin-disc stars and the SRMR stars continue to slowly decrease below [S/M] = 0 when [M/H] becomes positive. Then, most of the thin-disc stars have metallicity higher than −0.5 dex, although an extension can be seen down to [M/H] ∼ −0.9 dex. The thick-disc stars follow the slope of the green line, and are preferentially located ∼0.1 dex above it. Finally, potential halo stars are found down to [M/H] ∼ −2.0 dex. Their halo membership is confirmed by their rather low rotational velocities, as shown in the top panel of Fig. 6. Their [S/M] ratio is compatible with a flat behaviour (like any other α-element) and they have a mean [S/M] ratio close to +0.45 dex with a dispersion equal to 0.15 dex.

Moreover, we also show in the middle panel of Fig. 8 the stars with Mg abundances from Santos-Peral et al. (2020a), already shown in Fig. 4. They are drawn according to their Galactic population membership as defined by their sulfur abundances. It can be seen that (i) the thin-disc/sulfur-poor stars are the most magnesium poor, (ii) most of the SRMR stars are also magnesium-rich/metal-rich, and (iii) thick-disc/sulfur-rich stars tend also to have higher [Mg/M] ratios. There is only one halo star in this subsample, but its sulfur and magnesium enrichment are consistent. Therefore, although the scatter in sulfur appears larger than in magnesium, we can conclude that defining the Galactic populations from their [S/M] content would give results consistent with those obtained from most commonly used ratios, for instance [Mg/M].

4.5. Galactic radial gradients in sulfur

For the estimation of the Galactic gradient of sulfur for our ∼400 stars belonging to the thin disc, we considered the guiding centre radius (R_g), computed as the average of the pericentre and apocentre of the stellar orbits, as a proxy of the present star Galactocentric distance. The gradient (and associated uncertainty) was estimated thanks to a Theil-Sen fit of the [S/M] versus R_g points, the uncertainty being given by the lower and upper confidence levels of this fit. We find a small positive radial gradient $\delta[S/M]/\delta R_g = +0.004^{\pm 0.006}$ dex kpc^{-1} in the thin disc for R_g within 6 and 10 kpc. This gradient is slightly flatter than the [α/Fe] gradient of 0.012 ± 0.002 dex kpc^{-1} found between 5 and 13 kpc using *Gaia*-ESO Survey abundances (Recio-Blanco et al. 2014, but no *Gaia* distances were available at that time) and that of Santos-Peral et al. (2020a) estimated for magnesium over iron for AMBRE stars ($+0.025 \pm 0.009$ dex kpc^{-1} between 6 et 11 kpc). However, the Galactic (thin) disc gradient in sulfur has recently been estimated from 17 HII regions with revisited *Gaia* distances ranging between ∼7 and ∼14 kpc (Arellano-Córdova et al. 2020). This study reports a radial gradient in [S/H] equal to $-0.035^{\pm 0.006}$ dex kpc^{-1} in good agreement within the error bars with our determination: $\delta[S/H]/\delta R_g = -0.05^{\pm 0.025}$ dex kpc^{-1}. We also note that these authors found a flat gradient for [S/O], confirming independently the similar nature of these two chemical species, and hence the α nature of sulfur.

We also computed the radial gradient in the thick disc between 4.5 and 15.5 kpc: $\delta[S/M]/\delta R_g = -0.014^{\pm 0.014}$ dex kpc^{-1}, in agreement within the error bars with the value reported by Recio-Blanco et al. (2014, -0.004 ± 0.003 dex within 4 and

11 kpc). Adding the SRMR stars to the thick-disc sample (leading to a total of ∼150 stars) would not change this sulfur-to-mean metallicity radial gradient since we found $-0.01^{\pm-0.015}$ dex kpc^{-1}.

5. Summary

We have presented LTE sulfur abundances derived from the three main components of the multiplet 8 system lines found around 675 nm, which are known to be poorly affected by NLTE effects. This study analysed ∼100 000 spectra (including several repeats per stars) retrieved from the ESO archives of the HARPS, FEROS, and UVES instruments. These sulfur abundances have been homogeneously measured at a spectral resolution of 40 000 thanks to (i) stellar atmospheric parameters previously determined within the AMBRE Project (de Laverny et al. 2013); (ii) GAUGUIN, an optimisation method based on the Gauss-Newton algorithm; and (iii) a precomputed grid of synthetic spectra with [S/H] abundances varying from −3.0 to +2.0 dex. Then, each spectrum with at least one measured SI line has been considered to derive a mean sulfur abundance per star and an associated dispersion, based on the line-to-line scatter and the available repeat spectra. The final catalogue contains abundances for 1855 individual slow-rotating stars. About 90% of the sample consists of FGK-dwarf stars and the remaining 10% are cool giants. Their mean metallicity is between −2.0 to +0.7 dex. This is the largest catalogue of accurate and precise sulfur abundances published to date. We also present sulfur abundances of 13 *Gaia* benchmark stars re-estimated by considering their recommended stellar parameters.

This AMBRE-sulfur catalogue allowed us to study the origin and evolution of sulfur in the Milky Way. First, we have shown that sulfur presents behaviours that are close to any other α-element. The mean [S/M] is equal to ∼0.45 dex for [M/H] < −1.0 dex and the distribution of [S/M] is compatible with a plateau-like behaviour in the low-metallicity regime. Then, a monotonic decline is found with increasing metallicity. Moreover, this decline clearly continues for supersolar metallicity (without any slope change), as already independently found for AMBRE magnesium abundances (Santos-Peral et al. 2020a). All of this is also confirmed by the low [S/α] ratios found over the whole studied metallicity range and by the similar behaviour of our sulfur abundances with metallicity compared to previous magnesium and europium abundances, both elements being predominantly produced by Type II supernovae (although still discussed for europium).

Then, thanks to *Gaia* DR2 astrometry, we have studied the correlation between the AMBRE-sulfur abundances and the stellar kinematic and orbital properties. A dichotomy in kinematics and eccentricity is detected between sulfur-rich and sulfur-poor stars at metallicities lower than ∼ −0.5 dex. Two disc components that could be associated with the thin and the thick discs, with different sulfur content and kinematical properties are also identified. We have then proposed that the thin-disc/thick-disc dichotomy could be defined by solely considering sulfur abundances, as done in previous studies by considering any other α-species. Furthermore, a trend with small dispersion between stellar ages and sulfur content is found: [S/M] slowly increases with stellar age up to ∼11 Gyr, whereas the metallicity decreases and then a much steeper slope appears for older more metal-poor stars. Sulfur could thus be used as a chemical clock, although some dispersion could appear when examining a larger sample. Finally, we have estimated the sulfur radial gradient in the thin disc and found a small positive gradient for δ[S/M]/δR_g consistent with previous studies, in particular the gradient derived from the sulfur content of HII regions. The gradient in the thick disc is found to be slightly smaller.

This work therefore proposes that the Galactic chemical history of sulfur is similar to that of a typical α-element, and that this chemical species could be adopted with confidence to study Galactic stellar populations.

Acknowledgements. We are grateful to Robin Bonannini who starts a preliminary study of sulfur abundances with AMBRE data several years ago. This work has made use of data from the European Space Agency (ESA) mission *Gaia* (https://www.cosmos.esa.int/gaia), processed by the *Gaia* Data Processing and Analysis Consortium (DPAC, https://www.cosmos.esa.int/web/gaia/dpac/consortium). Funding for the DPAC has been provided by national institutions, in particular the institutions participating in the *Gaia* Multilateral Agreement. This research has also made use of the SIMBAD database, operated at CDS, Strasbourg, France. The authors acknowledge financial support from the ANR 14-CE33-014-01. This work was also supported by the "Programme National de Physique Stellaire" (PNPS) of CNRS/INSU co-funded by CEA and CNES. M. A. A. acknowledges support from the CIGUS -CITIC, funded by Xunta de Galicia and the European Union (FEDER Galicia 2014-2020 Program) by grant ED431G 2019/01. Finally, most of the calculations have been performed with the high-performance computing facility SIGAMM, hosted by OCA.

References

Adibekyan, V. Z., Santos, N. C., Sousa, S. G., & Israelian, G. 2011, A&A, 535, L11
Adibekyan, V. Z., Sousa, S. G., Santos, N. C., et al. 2012, A&A, 545, A32
Adibekyan, V., Figueira, P., Santos, N. C., et al. 2015, A&A, 583, A94
Amarsi, A. M., Lind, K., Osorio, Y., et al. 2020, A&A, 642, A62
Arellano-Córdova, K. Z., Esteban, C., García-Rojas, J., & Méndez-Delgado, J. E. 2020, MNRAS, 496, 1051
Bailer-Jones, C. A. L., Andrae, R., Arcay, B., et al. 2013, A&A, 559, A74
Bailer-Jones, C. A. L., Rybizki, J., Fouesneau, M., Mantelet, G., & Andrae, R. 2018, AJ, 156, 58
Bensby, T., Feltzing, S., & Lundström, I. 2003, A&A, 410, 527
Biemont, E., Quinet, P., & Zeippen, C. J. 1993, A&AS, 102, 435
Bijaoui, A., Recio-Blanco, A., de Laverny, , & Ordenovic, C. 2010, in ADA 6 - Sixth Conference on Astronomical Data Analysis, 9
Bijaoui, A., Recio-Blanco, A., de Laverny, P., & Ordenovic, C. 2012, Stat. Methodol., 9, 55
Bovy, J. 2015, ApJS, 216, 29
Caffau, E., Bonifacio, P., Faraggiana, R., et al. 2005, A&A, 441, 533
Chen, Y. Q., Nissen, P. E., Zhao, G., & Asplund, M. 2002, A&A, 390, 225
Cleveland, W. S. 1979, J. Am. Stat. Assoc., 74, 829
Costa Silva, A. R., Delgado Mena, E., & Tsantaki, M. 2020, A&A, 634, A136
de Laverny, P., Recio-Blanco, A., Worley, C. C., & Plez, B. 2012, A&A, 544, A126
de Laverny, P., Recio-Blanco, A., Worley, C. C., et al. 2013, Messenger, 153, 18
De Pascale, M., Worley, C. C., de Laverny, P., et al. 2014, A&A, 570, A68
Duffau, S., Caffau, E., Sbordone, L., et al. 2017, A&A, 604, A128
Francois, P. 1988, A&A, 195, 226
Gaia Collaboration (Brown, A. G. A., et al.) 2018, A&A, 616, A1
Gazzano, J. C., Kordopatis, G., Deleuil, M., et al. 2013, A&A, 550, A125
Gilmore, G., & Reid, N. 1983, MNRAS, 202, 1025
Grevesse, N., Asplund, M., & Sauval, A. J. 2007, Space Sci. Rev., 130, 105
Grisoni, V., Spitoni, E., Matteucci, F., et al. 2017, MNRAS, 472, 3637
Guiglion, G., de Laverny, P., Recio-Blanco, A., et al. 2016, A&A, 595, A18
Guiglion, G., de Laverny, P., Recio-Blanco, A., & Prantzos, N. 2018, A&A, 619, A143
Gustafsson, B., Edvardsson, B., Eriksson, K., et al. 2008, A&A, 486, 951
Hayden, M. R., Bovy, J., Holtzman, J. A., et al. 2015, ApJ, 808, 132
Hayden, M. R., Recio-Blanco, A., de Laverny, P., Mikolaitis, S., & Worley, C. C. 2017, A&A, 608, L1
Heiter, U., Lind, K., Bergemann, M., et al. 2021, A&A, 645, A106
Henden, A. A., Levine, S., Terrell, D., et al. 2018, in American Astronomical Society Meeting Abstracts #232, Am. Astron. Soc. Meeting Abstr., 232, 223.06
Israelian, G., & Rebolo, R. 2001, ApJ, 557, L43
Jofré, P., Heiter, U., Tucci Maia, M., et al. 2018, Res. Notes Am. Astron. Soc., 2, 152
Kacharov, N., Koch, A., Caffau, E., & Sbordone, L. 2015, A&A, 577, A18
Kobayashi, C., Karakas, A. I., & Umeda, H. 2011, MNRAS, 414, 3231

Kobayashi, C., Karakas, A. I., & Lugaro, M. 2020, ApJ, 900, 179
Kordopatis, G., Amorisco, N. C., Evans, N. W., Gilmore, G., & Koposov, S. E. 2016, MNRAS, 457, 1299
Kordopatis, G., Wyse, R. F. G., Chiappini, C., et al. 2017, MNRAS, 467, 469
Korotin, S. A. 2009, Astron. Rep., 53, 651
Korotin, S., Andrievsky, S., Caffau, E., & Bonifacio, P. 2017, in Stars: From Collapse to Collapse, eds. Y. Y. Balega, D. O. Kudryavtsev, I. I. Romanyuk, & I. A. Yakunin, ASP Conf. Ser., 510, 141
Luck, R. E. 2015, AJ, 150, 88
Matrozis, E., Ryde, N., & Dupree, A. K. 2013, A&A, 559, A115
Mikolaitis, Š., Hill, V., Recio-Blanco, A., et al. 2014, A&A, 572, A33
Mikolaitis, Š., de Laverny, P., Recio-Blanco, A., et al. 2017, A&A, 600, A22
Nissen, P. E., Chen, Y. Q., Asplund, M., & Pettini, M. 2004, A&A, 415, 993
Nissen, P. E., Akerman, C., Asplund, M., et al. 2007, A&A, 469, 319
Nomoto, K., Kobayashi, C., & Tominaga, N. 2013, ARA&A, 51, 457
Palla, M., Matteucci, F., Spitoni, E., Vincenzo, F., & Grisoni, V. 2020, MNRAS, 498, 1710
Plez, B. 2012, Turbospectrum: Code for Spectral Synthesis (Astrophysics Source Code Library)
Prantzos, N., Abia, C., Limongi, M., Chieffi, A., & Cristallo, S. 2018, MNRAS, 476, 3432
Recio-Blanco, A., Bijaoui, A., & de Laverny, P. 2006, MNRAS, 370, 141
Recio-Blanco, A., de Laverny, P., Kordopatis, G., et al. 2014, A&A, 567, A5
Recio-Blanco, A., de Laverny, P., Allende Prieto, C., et al. 2016, A&A, 585, A93
Reddy, B. E., Lambert, D. L., & Allende Prieto, C. 2006, MNRAS, 367, 1329
Romano, D., Karakas, A. I., Tosi, M., & Matteucci, F. 2010, A&A, 522, A32
Ryde, N. 2006, A&A, 455, L13
Ryde, N., & Lambert, D. L. 2004, A&A, 415, 559
Santos-Peral, P., Recio-Blanco, A., de Laverny, P., Fernández-Alvar, E., & Ordenovic, C. 2020a, A&A, 639, A140
Santos-Peral, P., Recio-Blanco, A., Kordopatis, G., et al. 2020b, A&A, submitted
Savage, B. D., & Sembach, K. R. 1996, ARA&A, 34, 279
Schönrich, R., Binney, J., & Dehnen, W. 2010, MNRAS, 403, 1829
Scott, P., Grevesse, N., Asplund, M., et al. 2015, A&A, 573, A25
Skrutskie, M. F., Cutri, R. M., Stiening, R., et al. 2006, AJ, 131, 1163
Spite, M., Caffau, E., Andrievsky, S. M., et al. 2011, A&A, 528, A9
Takeda, Y., Omiya, M., Harakawa, H., & Sato, B. 2016, PASJ, 68, 81
Wallace, L., Hinkle, K. H., Livingston, W. C., & Davis, S. P. 2011, ApJS, 195, 6
Wiese, W. L., Smith, M. W., & Miles, B. M. 1969, Atomic Transition Probabilities. Vol. 2: Sodium Through Calcium. A Critical Data Compilation
Woosley, S. E., & Weaver, T. A. 1995, ApJS, 101, 181
Worley, C. C., de Laverny, P., Recio-Blanco, A., et al. 2012, A&A, 542, A48
Worley, C. C., de Laverny, P., Recio-Blanco, A., Hill, V., & Bijaoui, A. 2016, A&A, 591, A81
Yoshii, Y. 1982, PASJ, 34, 365